Journal of Catalysis **197,** 292–302 (2001)
doi:10.1006/jcat.2000.3063, available online at http://www.idealibrary.com on IDEAL®

Catalytic Decomposition of 2-Propanol over Different Metal-Cation-Doped OMS-2 Materials

Xiao Chen,* Yan-Fei Shen,*,[1] Steven L. Suib,*,†,‡,[2] and C. L. O'Young§

*Department of Chemistry and †Department of Chemical Engineering, ‡Institute of Materials Science, University of Connecticut, Storrs, Connecticut 06269; and §Texaco Research Center, Texaco, Inc., P.O. Box 509, Beacon, New York 12508

Received July 16, 2000; revised October 3, 2000; accepted October 3, 2000; published online January 5, 2001

The catalytic properties of manganese oxide octahedral molecular sieve materials (OMS-2) with different metal cation dopants (*M*: Cu^{2+}, Zn^{2+}, Ni^{2+}, Co^{2+}, Al^{3+}, or Mg^{2+}) were investigated for the reaction of 2-propanol decomposition. Compared with other *M*–OMS-2 catalysts, Cu–OMS-2 catalyst has much higher conversion of 2-propanol and the highest selectivity to acetone at 300°C. As for the selectivity to propene, it is generally below 6% for *M*–OMS-2 materials. The reaction results are discussed in consideration of characterization results of *M*–OMS-2 catalysts, especially studies on their acidity and basicity, and suggest that dehydrogenation of 2-propanol is not simply catalyzed by basic or acidic and basic pair sites, but probably by active sites with redox and basic properties. *In situ* FTIR studies suggest that Cu–OMS-2 has more active sites for 2-propanol than Al–OMS-2 and K–OMS-2. The phase transitions from cryptomelane to hausmannite and finally to manganosite were observed with XRD studies of Cu–OMS-2 catalysts during reaction. All Cu–OMS-2 materials that either have the cryptomelane, amorphous MnO_y, hausmannite, or manganosite structure show activity in the decomposition of 2-propanol to acetone. The Cu–OMS-2 materials with the hausmannite structure show the highest activity.

I. INTRODUCTION

Decomposition of 2-propanol has been frequently used as a test reaction for acid–base properties of oxide catalysts (1–15). Decomposition of 2-propanol occurs by two parallel reactions: (1) dehydration to propene predominantly on acid sites and (2) dehydrogenation to acetone on basic or concerted acid–base pair sites or on active sites with redox and basic properties. However, the role of acidic and basic sites in the formation of propene and acetone is not well established (1, 16). Recent reports (17, 18) show that dehydrogenation and dehydration of 2-propanol are not only determined by surface acidic or basic properties but also strongly affected by the reaction conditions employed, such as reaction temperature, 2-propanol partial pressure, the oxidizing nature of the carrier gas, and so forth.

The reaction of 2-propanol decomposition was chosen to test the catalytic property of manganese nodules by Matsuo *et al.* (19, 20). Their reaction products were acetone, carbon dioxide, and water, but no propene was detected. Surface oxygen species on the manganese nodule surface were believed to act as basic sites to catalyze the dehydrogenation of 2-propanol. Some of the surface oxygen species were highly reactive so that the total oxidation of 2-propanol occurred. The acidity on the manganese nodule surface was postulated to be too weak to catalyze the dehydration of 2-propanol.

A new class of molecular sieve materials referred to as manganese oxide octahedral molecular sieves (OMS), including synthetic todorokite (OMS-1) and cryptomelane (OMS-2), has been developed (21–27). The synthesis, characterization, and potential applications of OMS materials have been reported in the literature (21–27). Most of the literature focuses on the description of the materials themselves while fewer attempts have been made in the area of catalytic applications of OMS materials.

OMS materials have been found effective in the total oxidation of carbon monoxide (28, 29), decomposition of H_2O_2 (30), oxidative dehydrogenation of ethanol (31), and liquid-phase dehydrogenation of cyclohexane to cyclohexene (32). In oxidative dehydrogenation of 1-butene at 450°C, phase changes from the original phase of OMS materials to a mixture of Mn_3O_4/MnO or pure MnO were found, indicating that OMS materials are not stable under reducing conditions at high temperatures (33).

In this research, the decomposition of 2-propanol on different metal- (*M*-) cation-doped manganese oxide octahedral molecular sieve materials (which are referred to as *M*–OMS-2 materials (34)) is studied to investigate the influence of metal dopants on the catalytic properties of OMS-2-type materials. The catalytic results are discussed and related to the characterization results of *M*–OMS-2 materials (34), such as structural, chemical composition, surface, and textural properties. Phase transitions and

[1] Current address: The Gillette Company, North Atlantic Group, One Gillette Park, Boston, MA 02127-1096.

[2] To whom correspondence should be addressed.

0021-9517/01 $35.00

adsorbed species on Cu–OMS-2 materials during the decomposition of 2-propanol were monitored with X-ray powder diffraction (XRD) and Fourier transform infrared spectroscopy (FTIR), respectively. The results are correlated with the unique catalytic behavior of Cu–OMS-2 materials in the reaction.

II. EXPERIMENTAL

2.1. Synthesis of M–OMS-2 Materials

M–OMS-2 materials were prepared by using reflux methods after the oxidation of Mn^{2+} by $KMnO_4$. Metal (*M*) cations (Cu^{2+}, Zn^{2+}, Ni^{2+}, Co^{2+}, Al^{3+}, or Mg^{2+}) were doped into the OMS-2 structure by adding aqueous solutions of dopant before reflux. The details of these preparations are given in the literature (22–26). OMS-2 materials were prepared by oxidation of Mn^{2+} by permanganate with refluxing. Typically, 13.3 g of $KMnO_4$ dissolved in 225 mL of water was added to a solution of 19.8 g of $MnSO_4 \cdot H_2O$ in 67.5 mL of water and 6.8 mL of concentrated nitric acid. Refluxing took place for up to 24 h. The product was filtered, washed seven times with distilled deionized water, and dried at 120°C overnight.

Doping of the OMS-2 samples was done by adding transition-metal nitrate salts to the $KMnO_4$ and Mn^{2+} mixed solutions prior to mixing. Various amounts, such as 1.5, 13.0, and 26.0 mL, of 1.0 M $Cu(NO_3)_2 \cdot 6H_2O$ solutions were added to prepare different dopant levels of copper in OMS-2. Resultant materials were filtered, washed, and dried as with nondoped materials.

2.2. Characterization of M–OMS-2 Materials

X-ray diffraction (XRD) patterns of samples before and after reaction were collected by using a Scintag 2000 XDS diffractometer with Cu$K\alpha$ X-ray radiation at a beam voltage of 45 kV and beam current of 40 mA. A 0.02 step in 2θ/count was used to collect these XRD patterns.

Inductively coupled plasma-atomic emission spectroscopy (ICP-AES) was employed for elemental composition analyses for potassium, manganese, and other metal cations of *M*–OMS-2 materials. A Perkin–Elmer 7-40 instrument equipped with an autosampler was used to carry out the analyses at the Environmental Research Institute, Storrs, CT.

2.3. Decomposition of 2-Propanol over M–OMS-2 Materials

The reaction of 2-propanol decomposition was carried out in a $\frac{1}{4}$-in. (i.d.) tubular glass flow reactor with a loading of 22 mg of prepared *M*–OMS-2 materials, which have a particle size of 28–48 mesh (300–590 μm). The *M*–OMS-2 materials were pretreated at 1 atm and 300°C for 1 h in He with a flow rate of 30 mL/min. To carry out the decomposition, 2-propanol vapor was fed into the reactor by passing He through a 2-propanol bubbler at 22°C at a flow rate of 6 mL/min. The reaction conditions were 1 atm and 300°C. The products were analyzed with an on-line HP 5880A series gas chromatograph (GC) with a Carbowax column.

2.4. In Situ FTIR Studies of the Adsorption of 2-Propanol over M–OMS-2 Materials

The *in situ* FTIR spectra were obtained on a Nicolet Magna-IR Spectrometer 750 equipped with an *in situ* high-temperature cell for heating, adsorption, and reaction. Standard procedures of single-beam diffuse reflectance methods with an MCT-B detector and a KBr beam splitter were applied to collect IR spectra of samples. For all IR spectra, 200 scans were taken with a resolution of 4 cm^{-1}.

The *in situ* FTIR studies were conducted by collecting IR spectra of Cu–OMS-2-I, Al–OMS-2, or OMS-2 at different stages with the following procedures. Fine powders of the examined sample were placed in the *in situ* cell and pretreated at 120°C under a He stream (20 mL/min) for 3 h. The He stream was then switched to pass through a 2-propanol bubbler at 22°C to introduce 2-propanol vapor into the *in situ* cell for 0.5 h. The He plus 2-propanol stream was then switched back to He to purge unadsorbed or weakly adsorbed 2-propanol in the *in situ* cell for 3 h. The *in situ* cell was heated to 200 and 270°C consecutively and kept at each temperature for 0.5 h under He.

III. RESULTS

3.1. Characterization of M–OMS-2 Materials

XRD patterns for fresh OMS-2 and reference patterns for synthetic cryptomelane (KMn_8O_{16}) from JCPDS 29,1020 are shown in Fig. 1. All other synthesized *M*–OMS-2 samples have XRD patterns similar to those of OMS-2. This indicates that all synthesized *M*–OMS-2 materials have a cryptomelane-type structure. The results of ICP-AES elemental analyses for cations in all synthesized *M*–OMS-2 materials are summarized in Tables 1 and 2.

3.2. Decomposition of 2-Propanol over M–OMS-2 Materials

3.2.1. Effects of different M dopants. Effects of different *M* dopants on the conversion of 2-propanol at 300°C are

TABLE 1

ICP-AES Elemental Analysis Results of Cu–OMS-2 Materials

Materials	Cu–OMS-2-I	Cu–OMS-2-II	Cu–OMS-2-III	Cu–OMS-2-IV
Cu (mol/100 g[a])	0.056	0.050	0.041	0.018
K (mol/100 g[a])	0.086	0.093	0.099	0.115
Mn (mol/100 g[a])	1.133	1.106	1.120	1.148

[a] With respect to 100 g of material.

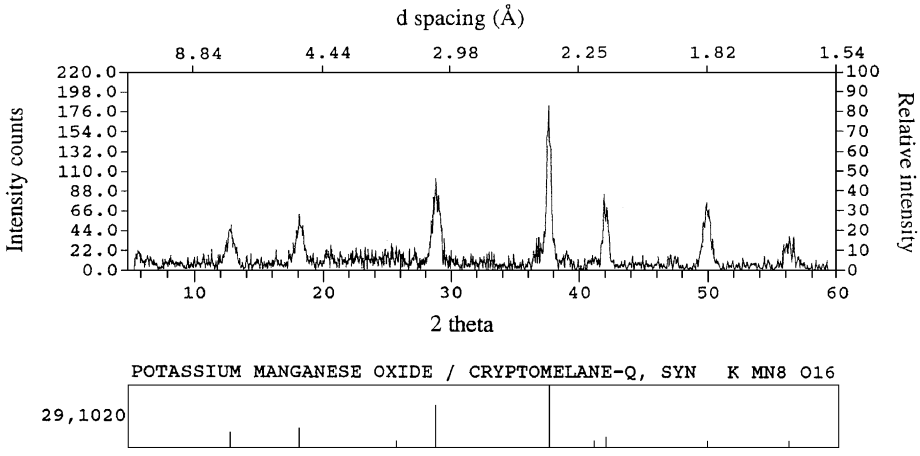

FIG. 1. XRD pattern of fresh OMS-2 (top) and reference pattern for synthetic cryptomelane (KMn_8O_{16}) from JCPDS 29,1020 (bottom).

shown in Fig. 2a. Cu–OMS-2 has much higher activity in the reaction of 2-propanol decomposition than other *M*–OMS-2 materials.

Figure 2b shows the effects of different *M* dopants on selectivities of 2-propanol decomposition at 300°C. The major product of the reaction in 2-propanol over *M*–OMS-2 materials is acetone, which has selectivities generally greater than 89%. One of the other minor products is propene. The selectivities to propene for the reaction of 2-propanol over *M*–OMS-2 materials are below 6%, as shown in Fig. 2b. Al–OMS-2 material has the highest selectivity to propene (6%). CO_2 was also detected during the reaction of 2-propanol over *M*–OMS-2 materials with selectivities less than 10%. The reaction of 2-propanol on *M*–OMS-2, therefore, leads to the decomposition of 2-propanol to acetone, propene, and CO_2. If only acetone and propene are considered, the relative selectivities to acetone are greater than 94%, as indicated by the Acet/(Acet + Prop) ratio in Fig. 2b.

3.2.2. Effects of Cu dopant content. Effects of Cu dopant content in Cu–OMS-2 materials in the decomposition of 2-propanol at 300°C were also studied. The results are shown in Fig. 3. The conversion of 2-propanol increases with increasing Cu content of Cu–OMS-2 materials.

Figure 3b shows effects of Cu-dopant content in Cu–OMS-2 materials on the selectivities of 2-propanol decomposition at 300°C. The major product of the reaction of 2-propanol over Cu–OMS-2 materials is also acetone with selectivities greater than 96%. The selectivities to propene in the reaction of 2-propanol over Cu–OMS-2 materials are below 2%, as shown in Fig. 3b. If only acetone

TABLE 2

ICP-AES Elemental Analysis Results of *M*–OMS-2 Materials

M	OMS-2	Mg	Ni	Al	Zn	Co
M (mol/100 g[a])	0	0.005	0.017	0.022	0.023	0.085
K (mol/100 g[a])	0.115	0.105	0.100	0.099	0.098	0.098
Mn (mol/100 g[a])	1.300	0.945	0.910	0.949	0.917	0.874

[a] With respect to 100 g of material.

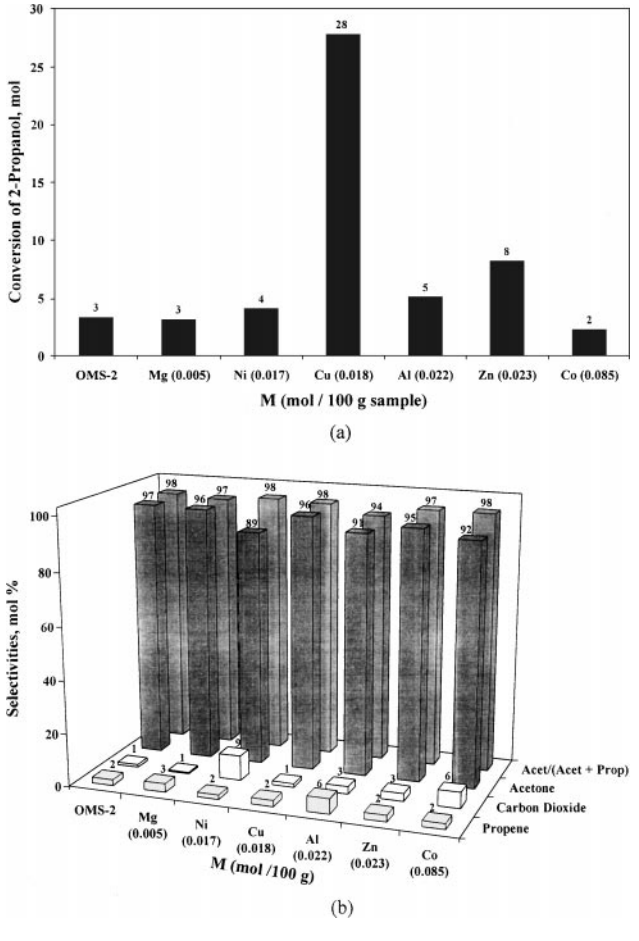

FIG. 2. Effects of different *M* dopants on (a) the conversion of 2-propanol and (b) the selectivities of 2-propanol decomposition at 300°C.

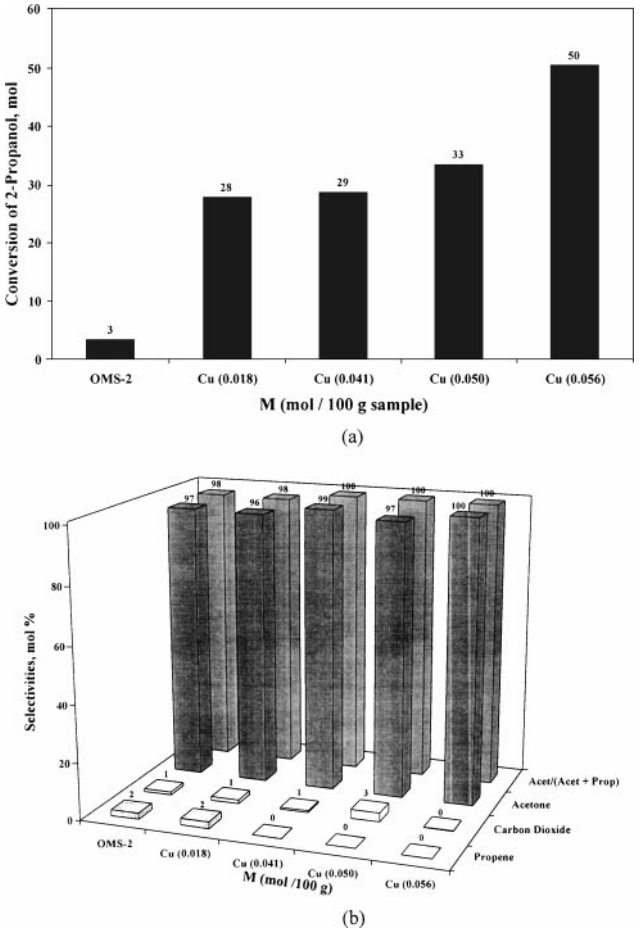

FIG. 3. Effects of Cu dopant content in Cu–OMS-2 materials on (a) the conversion of 2-propanol and (b) the selectivities of 2-propanol decomposition at 300°C.

and propene are considered, the selectivities to acetone are greater than 98%, as indicated by the Acet/(Acet + Prop) ratio in Fig. 3b. When the Cu content in Cu–OMS-2 materials is higher than 0.041 mol/100 g of materials, no propene is detected in the products. CO_2 was also detected during the reaction of 2-propanol over Cu–OMS-2 materials with selectivities less than 3%.

3.2.3. XRD pattern of M–OMS-2 materials after the reaction of 2-propanol decomposition. Figure 4 shows the XRD pattern for OMS-2 after the reaction of 2-propanol decomposition and the reference pattern for synthetic manganosite (manganese oxide: MnO) from JCPDS 7,230. All other *M*–OMS-2 materials have XRD patterns similar to that of OMS-2 after the reaction. This indicates that all synthesized *M*–OMS-2 materials have changed to a manganosite-type structure after reaction.

3.3. XRD Study of the Phase Transition of Cu–OMS-2 Materials during the Reaction of 2-Propanol Decomposition

Two long time reaction runs on the decomposition of 2-propanol were carried out over Cu–OMS-2-I at two different temperatures, 200 and 300°C. The conversion of 2-propanol versus reaction time is shown in Fig. 5a. Figure 5b shows the selectivity to acetone versus reaction time for those two runs, during which CO_2 was detected as another product but no propene was found.

To monitor the crystal-phase change of Cu–OMS-2-I during the reaction, five more runs were performed for different times on stream (TOS) at 300°C and four runs at 200°C. The results of those repeated runs are consistent with the results of the long time runs. Each reaction run was stopped by switching the feed gas into the reactor from the reactant gas of 2-propanol vapor in helium to pure helium gas. Meanwhile, the reactor was cooled down to room temperature in air. After the reaction was stopped, Cu–OMS-2-I material was recovered and its XRD pattern was collected. All the XRD patterns are summarized in Figs. 6 and 7 for Cu–OMS-2-I during the decomposition of 2-propanol at 300 and 200°C, respectively.

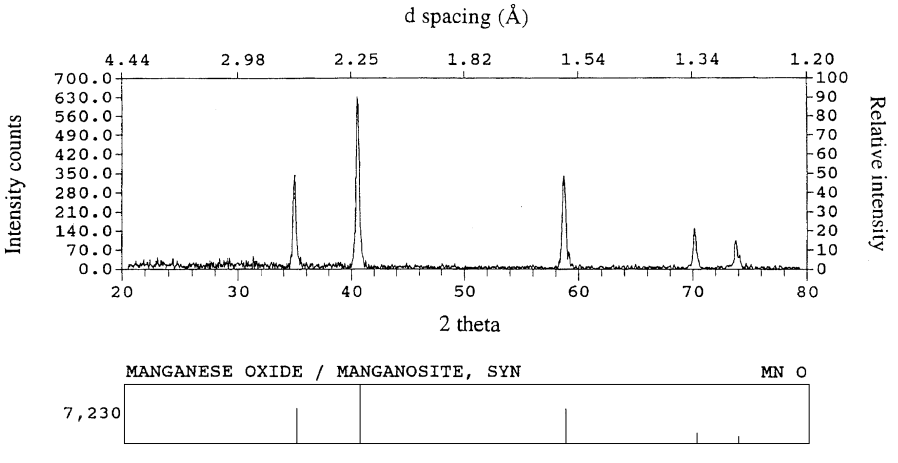

FIG. 4. The XRD pattern of OMS-2 after reaction and the reference pattern for synthetic manganosite.

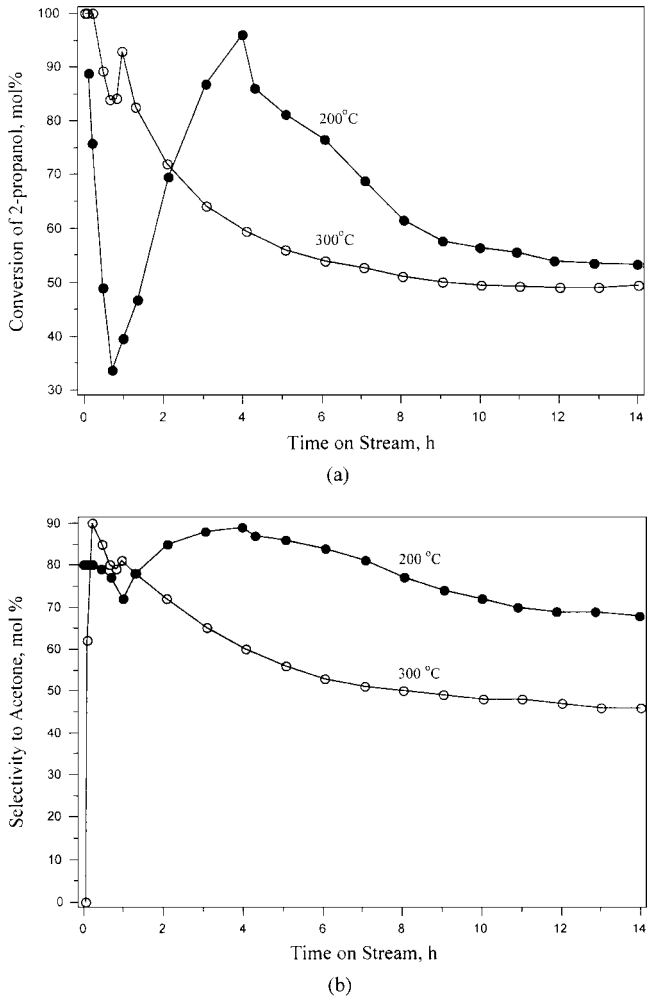

FIG. 5. Effects of different reaction temperatures on (a) the conversion of 2-propanol and (b) the selectivity to acetone over Cu–OMS-2-I.

3.3.1. Correlation of reaction results and phase changes at 300°C. The conversion of 2-propanol over Cu–OMS-2-I at 300°C is very high (100%) for the first 15 min of reaction, as shown in Fig. 5 a. The conversion of 2-propanol and selectivity to CO_2 increase very quickly to almost 100% in 9 min, then the selectivity to CO_2 decreases rapidly to 10%, and the selectivity to acetone increases dramatically to 90% at 15 min. However, the conversion of 2-propanol is still almost 100%. XRD patterns c and d in Figure 6 suggest that, after a very short time of reaction, such as 9 min, the cryptomelane structure in the Cu–OMS-2-I has transformed to hausmannite. The reaction and phase change results show that the cryptomelane structure in Cu–OMS-2-I has been reduced to hausmannite in a very short time and 2-propanol itself has been oxidized to CO_2. Meanwhile, Cu–OMS-2-I with the hausmannite structure shows high activity for the formation of acetone in the decomposition of 2-propanol.

After 15 min of reaction, the selectivity to CO_2 increases slowly to 19% in 1 h. The conversion of 2-propanol decreases from almost 100 to 89% in 30 min and then increases to 92% in 1 h. The XRD patterns e and f in Fig. 6 indicate that some hausmannite in Cu–OMS-2-I has been further reduced to manganosite (MnO) after 30 min of reaction and almost all of Cu–OMS-2-I changes to manganosite by 1 h.

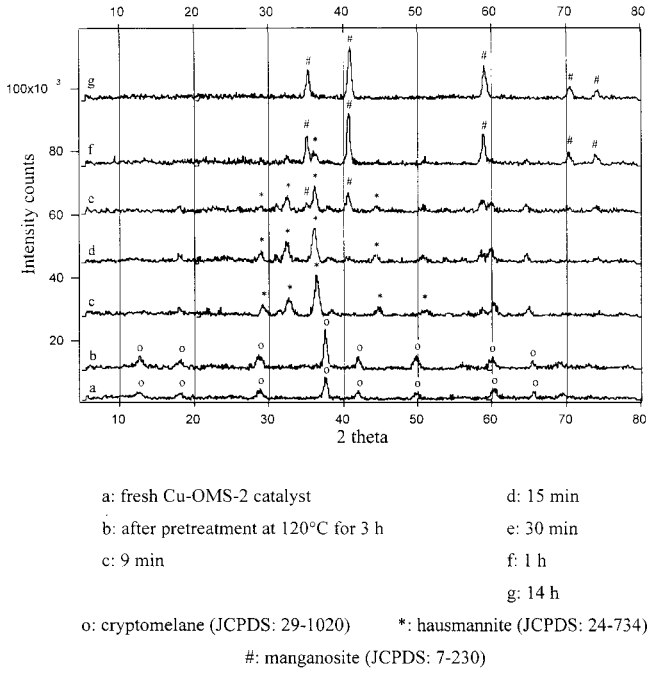

FIG. 6. XRD patterns of Cu–OMS-2-I before and during the decomposition of 2-propanol at 300°C.

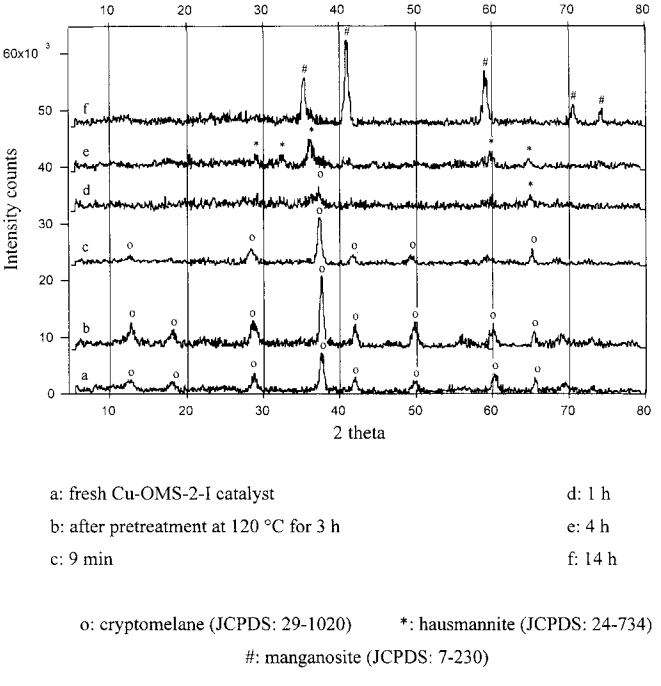

FIG. 7. XRD patterns of Cu–OMS-2-I before and during the decomposition of 2-propanol at 200°C.

After the selectivity to acetone reaches 81% at about 1 h, there is a slow decrease with increasing reaction time at 300°C, as shown in Fig. 5b. The conversion of 2-propanol also decreases in a similar way, as shown in Fig. 5a. These data suggest that the freshly formed manganosite also has high activity for producing acetone from the decomposition of 2-propanol, but the catalyst gradually deactivates later. The selectivity to CO_2 increases slowly when the conversion of 2-propanol and the selectivity to acetone decrease gradually after 1 h of reaction. This may be because there is still some amorphous MnO_y ($2 \leq y \leq 1$) in Cu–OMS-2-I after 1 h of reaction, although the XRD pattern (f in Fig. 6) shows that the sample has a manganosite structure with only a small amount of hausmannite. Amorphous MnO_y and a small amount of hausmannite in Cu–OMS-2-I can further oxidize 2-propanol to CO_2 at a relatively slower rate than α-MnO_2 in Cu–OMS-2-I after pretreatment at 120°C for 3 h.

The XRD pattern g in Fig. 6 indicates that the crystalline part of the converted Cu–OMS-2-I has the manganosite structure after 14 h of reaction. Even then, the material still has some activity for 2-propanol decomposition to acetone, as shown in Fig. 5.

BET surface areas of these materials are all near 250 m^2/g regardless of thermal treatment, dopants, or use in these reactions. There seems to be no correlation of activity and surface area in the catalytic decomposition of 2-propanol. We use the term activity as defined by sites per unit mass of catalyst.

3.3.2. The correlation between reaction results and phase changes at 200°C. At 200°C, the overall reaction behavior for 2-propanol decomposition over Cu–OMS-2-I and the phase transitions of Cu–OMS-2-I are similar to those at 300°C, although the transition rates are much slower than those at 300°C, as shown in Figs. 5–7. At the beginning of the reaction, the conversion of 2-propanol over Cu–OMS-2-I at 200°C is also high (80%), but lower than 100% at 300°C, as shown in Fig. 5a. However, the selectivity to acetone is 80% at 9 min at 200°C, compared to 0% at 300°C. XRD pattern c in Fig. 7 suggests that Cu–OMS-2-I still has the cryptomelane structure, but the amount of cryptomelane phase decreases after 9 min of reaction. This decrease is probably due to the reduction of some of the cryptomelane phase to amorphous MnO_y ($2 \leq y \leq 1$) by 2-propanol, which is oxidized to CO_2 at the same time.

After 9 min of reaction, the conversion of 2-propanol decreases from 89 to 39% in 1 h. The selectivity to acetone gradually decreases from 80 to 72% in 1 h and meanwhile the selectivity to CO_2 increases slowly from 20 to 28%. The XRD pattern d in Fig. 7 indicates that most of the Cu–OMS-2-I has been changed to an amorphous structure after 1 h of reaction. This is probably due to reduction of more cryptomelane phase to amorphous MnO_y by 2-propanol. All of the first hour of reaction results show that Cu–OMS-2-I with the cryptomelane structure has high activity for the formation of acetone in the decomposition of 2-propanol. The activity decreases when the cryptomelane phase is reduced and converted to amorphous MnO_y.

From 1 to 4 h of reaction, the conversion of 2-propanol gradually increases from 40 to 95% and the selectivity to acetone from 72 to 89%. The XRD pattern e in Fig. 7 indicates that after 4 h of reaction there is more hausmannite in Cu-OMS-2-I. This is probably due to the reduction of some amorphous MnO_y to hausmannite by 2-propanol. When the amount of hausmannite in Cu–OMS-2-I increases from the first to fourth hour of reaction, the activity and selectivity to acetone in the decomposition of 2-propanol also increase. The activity is even higher than that of Cu–OMS-2-I with the cryptomelane structure during the first 9 min of reaction at 200°C, showing that the activity and selectivity to acetone of hausmannite for 2-propanol decomposition are probably higher than those for cryptomelane.

After the conversion of 2-propanol and the selectivity to acetone reach their maxima at 4 h, they decrease slowly with increasing reaction time. From 4 to 14 h, the conversion and selectivity at 200°C are higher than those at 300°C. The XRD pattern f in Fig. 7 indicates that after 14 h of reaction most of the crystalline phase of Cu–OMS-2-I has changed to the manganosite structure, which is probably gradually produced by the reduction of hausmannite or amorphous MnO_y by 2-propanol. In a comparison of the XRD pattern f in Fig. 7 and the XRD pattern g in Fig. 6, the crystallites of manganosite in Cu–OMS-2-I after 14 h of reaction at 200°C are less crystalline than those at 300°C. The above results suggest that Cu–OMS-2-I with more crystalline manganosite has lower activity for producing acetone in the decomposition of 2-propanol, even at higher temperature.

3.4. In Situ FTIR Studies of the Adsorption of 2-Propanol over M–OMS-2 Materials

In situ FTIR study results of the adsorption of 2-propanol on Cu–OMS-2-I are shown in Fig. 8. The bands at about 755–770 and 660–670 cm^{-1} are characteristic of cryptomelane and involve the vibrations of the MnO_6 octahedral framework (35). Spectrum b for Cu–OMS-2-I during the introduction of 2-propanol at 120°C exhibits CH stretching bands (2980 and 2905 cm^{-1}) near 3000 cm^{-1} and a CH bending band (1383 cm^{-1}) of the 2-propyl group of adsorbed 2-propanol, as shown in Fig. 8. A band at 1128 cm^{-1} can be assigned to ν(C–O) of surface isopropoxide (11, 36), suggesting the presence of an adsorbed isopropoxide intermediate species on Cu–OMS-2-I, which may or may not be a real kinetically relevant intermediate. The bands at 1571 and 1443 cm^{-1} are probably due to acetate species. Surface acetate species display bands around 1550 and 1440 cm^{-1}, which have been assigned to asymmetric [ν_{as}(COO)] and symmetric [ν_s(COO)] stretching vibrations of acetate ions, respectively (11, 36).

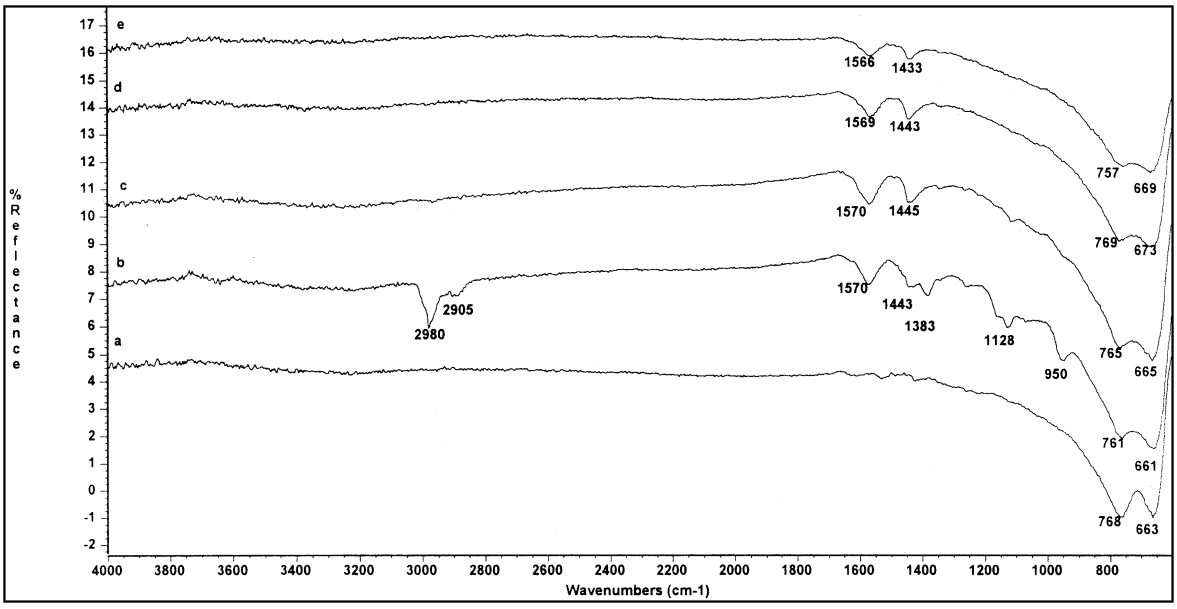

FIG. 8. IR spectra of Cu–OMS-2-I at different temperatures and in different atmospheres: (a) 120°C, He, before the introduction of 2-propanol; (b) 120°C, during the introduction of 2-propanol; (c) 120°C, He, after the introduction of 2-propanol; (d) 200°C, He, after the introduction of 2-propanol; (e) 270°C, He, after the introduction of 2-propanol.

After the unadsorbed or weakly adsorbed 2-propanol on the surface of Cu–OMS-2-I was purged by He at 120°C, all bands related to adsorbed 2-propanol disappeared except the bands around 1570 and 1440 cm^{-1}, which are related to acetate species, as shown in spectrum c of Fig. 8. As the temperature increased from 120 to 200°C, and further to 270°C, the intensities of the bands around 1570 and 1440 cm^{-1} decreased as well. This indicates that the amount of acetate species adsorbed on the surface of Cu–OMS-2-I was reduced at higher temperatures.

The IR spectra recorded after adsorption of 2-propanol on Al–OMS-2-I and OMS-2 are similar to each other, but quite different from those recorded for Cu–OMS-2-I. The IR spectra for Al–OMS-2 are shown in Fig. 9. Compared to spectrum b for Cu–OMS-2-I in Fig. 8, spectrum b for Al–OMS-2 during the introduction of 2-propanol at 120°C

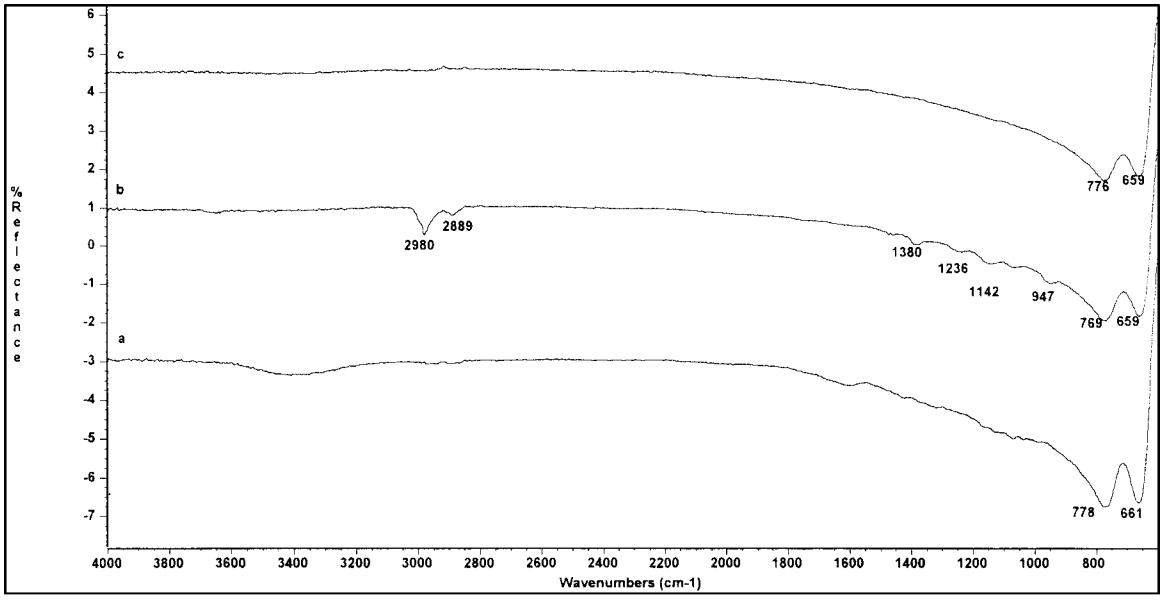

FIG. 9. IR spectra of Al–OMS-2 at different temperatures and in different atmospheres. (a) 120°C, He, before the introduction of 2-propanol; (b) 120°C, during the introduction of 2-propanol; (c) 120°C, He, after the introduction of 2-propanol.

exhibits CH stretching bands (2980 and 2889 cm^{-1}) of adsorbed 2-propanol with weaker intensities. The intensity of the CH bending band (1383 cm^{-1}) is even much weaker. No distinctive band at 1128 cm^{-1} has been observed for the ν(C–O) of surface isopropoxide. No stretching vibrational bands of acetate ions have been found around 1550 and 1440 cm^{-1}. After unadsorbed or weakly adsorbed 2-propanol species on the surface of Al–OMS-2 have been purged out by He at 120°C, no bands related to adsorbed 2-propanol were observed in spectrum c of Fig. 8.

In summary, more adsorbed 2-propanol species have been observed on Cu–OMS-2-I after the adsorption of 2-propanol than on Al–OMS-2 and OMS-2. This suggests that Cu–OMS-2-I has more surface active sites for the adsorption of 2-propanol than Al–OMS-2 and OMS-2.

IV. DISCUSSION

4.1. 2-Propanol Decomposition over M–OMS-2 Materials

DeGuzman *et al.* (24) showed that Mn atoms in *M*–OMS-2-type materials prepared by reflux methods have an average oxidation state of about 3.8 and are mostly in the Mn^{4+} state, with minor amounts in the Mn^{3+} state. Therefore, manganese ions in OMS-2-type materials should have redox properties, especially high oxidation activity similar to MnO_{2-x} materials ($x = 0$–0.3), which are generally active catalysts for oxidation reactions (15). The redox properties of manganese ions in *M*–OMS-2-type materials could contribute to the high selectivity to acetone in the decomposition of 2-propanol as shown in Fig. 2b. Even after a short time of reaction, MnO_{2-x} has been changed to MnO, as shown in Fig. 4, due to MnO having redox properties. This is probably the reason why these materials can retain their activity and selectivity to acetone in the decomposition of 2-propanol, even after MnO_{2-x} has been changed to MnO.

Among the different *M*-cation-doped *M*–OMS-2 materials, Cu–OMS-2 materials have much higher activity toward the decomposition of 2-propanol to acetone than other *M*–OMS-2 materials, as shown in Fig. 2. O'Young *et al.* also reported that Cu–OMS-1 has much higher activity toward the dehydrogenation of 2-propanol to acetone than other *M*–OMS-1 materials (37). If the reaction of dehydrogenation of 2-propanol to acetone is an indicator of basicity, as often suggested in the literature (4, 6–10, 12–14, 38), Cu–OMS-2 materials should have more and stronger surface basic sites than other *M*–OMS-2 materials. This is not the case because all *M*–OMS-2 materials have similar basicity, as suggested by TPD studies for adsorbed CO_2 (34). Even mass spectrometry (MS) monitored reaction results (39) suggest that commercial MgO does not show much higher activity toward the dehydrogenation of 2-propanol than *M*–OMS-2 materials, although MgO has much more and stronger basic sites on its surface, as indicated by the results of TPD studies for adsorbed CO_2 (34). In addition, although there are more very weak basic sites and moderate basic sites, but less strong basic sites on commercial γ-Al_2O_3 than those on *M*–OMS-2 materials (34), no activity toward the dehydrogenation on γ-Al_2O_3 was detected in the MS monitored reaction.

Copper oxides, such as CuO and Cu_2O, are effective for redox-type reactions, such as oxidation and dehydrogenation (15), and they are the active components of commercial 2-propanol dehydrogenation catalysts (40). This redox property of copper oxides could be helpful in improving the activity toward acetone in the decomposition of 2-propanol over Cu–OMS-2 materials, because Cu in Cu–OMS-2 materials can exist as copper oxides (CuO, Cu_2O). In addition, the high activity may also be due to more defects introduced by the distortion of CuO_6 octahedra in the framework of the cryptomelane structure in Cu–OMS-2 materials. Another possible reason is that 2-propanol may have easier access to Cu^{2+} than to other doped metal cations because more Cu^{2+} ions are probably in the tunnels of *M*–OMS-2 materials, as suggested by ICP-AES analysis results (34). *In situ* FTIR studies also suggest that Cu–OMS-2-I has more active sites for 2-propanol on its surface than on the surface of Al–OMS-2 and OMS-2.

The oxidation ability of Cu^{2+} is the highest among the metal cation dopants employed in this research because it has the highest standard reduction potential (E^0) for all metal cations shown in Table 3. This may also be related to the unique high activity of Cu–OMS-2 materials toward dehydrogenation of 2-propanol. Instead of the aqueous reduction potentials employed here, the reduction potentials of the cations in the solid state should be used. The research results of Owen and Kung (41) suggest that the order of reduction potentials of cations, such as Mg^{2+}, Zn^{2+}, Cr^{3+}, Ni^{2+}, and Cu^{2+}, in the oxide agrees with that in aqueous solution.

MS monitored reaction results (39) suggest that γ-Al_2O_3 shows much higher activity toward the dehydration of

TABLE 3

The Standard Reduction Potentials for Different Metal Cations (42)

Reaction	E^0, V
$Cu^{2+} + e \leftrightarrow Cu^{+}$	0.153
$Ni^{2+} + 2e \leftrightarrow Ni$	−0.257
$Co^{2+} + 2e \leftrightarrow Co$	−0.28
$Zn^{2+} + 2e \leftrightarrow Zn$	−0.7618
$Mg^{2+} + 2e \leftrightarrow Mg$	−1.185
$Al^{3+} + 3e \leftrightarrow Al$	−1.662
$K^{+} + 2e \leftrightarrow K$	−2.931

2-propanol than M-OMS-2 materials. TPD studies of adsorbed NH_3 indicate that γ-Al_2O_3 has much more and stronger acidic sites on its surface than *M*–OMS-2 materials (34). This is consistent with the general conclusion that acidic sites on catalyst surfaces catalyze the dehydration of 2-propanol. The reason for the low activities of γ-Al_2O_3 and MgO toward the dehydrogenation of 2-propanol is probably because they have very poor redox properties, which are considered to be necessary for the formation of acetone during the decomposition of 2-propanol (2, 43–45). However, a reviewer has suggested that the properties of alumina are irrelevant since Lewis acid sites will be occupied by hydroxyl groups during alcohol decomposition and are not accessible as catalytic sites.

In summary, the reaction results in this research are consistent with the general idea that dehydration of 2-propanol occurs on acidic centers and dehydrogenation on acid–base pair sites or redox centers. Therefore, 2-propanol dehydrogenation to acetone is not a good test reaction for studying basicity. The redox properties of those materials may play a more important role in the dehydrogenation of 2-propanol.

CO_2 was detected during the reaction of 2-propanol over *M*–OMS-2 materials as shown in Figs. 2 and 3. The oxygen in CO_2 can only come from *M*–OMS-2 materials and 2-propanol because there is no other source of oxygen in the reaction system. The selectivities to CO_2 are generally very high at the beginning of the reaction. This is probably because of the initial total oxidation of 2-propanol by the very active dioxygen species adsorbed on the surface of *M*–OMS-2 materials, which is evidenced by the weak and broad desorption peak of O_2 in TPD studies of OMS-2 (34).

With increasing reaction time, CO_2 is produced continuously, although the selectivity is lowered due to less available active oxygen in the OMS-2 materials. Although oxygen in OMS-2 materials is limited, CO_2 is produced continuously during the 3 h of reaction because the flow rate of 2-propanol in the inlet gas to the reactor is very small ($\sim$0.2 mL of vapor/min at 22°C) and the conversion of 2-propanol is generally low (less than 10%), except for those of Cu–OMS-2 materials on which the selectivity to CO_2 is also generally lower than those on other *M*–OMS-2 materials, as shown in Figs. 2 and 3. After *M*–OMS-2 materials lose some of their oxygen atoms, MnO_{2-x} changes to MnO, as shown in Fig. 4.

4.2. The Correlation between Reaction Results and Phase Transitions of Cu–OMS-2-I during 2-Propanol Decomposition

XRD studies of phase transitions of Cu–OMS-2-I during the reaction of 2-propanol decomposition at both 200 and 300°C show that the bulk structure of the material gradually changes from cryptomelane (KMn_8O_{16}) to hausmannite (Mn_3O_4) and finally to manganosite (MnO). The phase transition is very fast and is finished in about 1 h during the reaction at 300°C. Lowering the reaction temperature to 200°C brings about the phase transition much slower with the possible formation of amorphous MnO_y from cryptomelane. MnO_y then changes to hausmannite in about 4 h and finally to manganosite. All the Cu–OMS-2 materials that either have the cryptomelane, amorphous MnO_y, hausmannite, or manganosite structure show activity in the decomposition of 2-propanol to acetone. The Cu–OMS-2 material containing the hausmannite structure shows the highest activity, although it is not stable under reaction conditions, as shown by reaction results at both 200 and 300°C. Copper oxides also show some activity but considerably less than the Cu–OMS-2 systems.

Similar phase transitions for Cu–OMS-2 during the oxidative dehydrogenation of 1-butene were observed by Krishnan and Suib (33). The final phase of their catalyst is a mixture of hausmannite and manganosite after 2 h of reaction with a feed of 1% 1-butene/0.7% O_2/argon at 450°C. A phase transition was proposed as follows,

$$\text{OMS-1/OMS-2} \rightarrow Mn_3O_4 \rightarrow \text{MnO},$$

corresponding to the redox scheme of general oxidation catalysis proposed by Mars and van Krevelen (46) and reviewed by Kung and Kung (47),

$$\text{A} \rightleftharpoons \text{B} \rightarrow \text{C},$$

where A, B, and C are different phases of an oxidation catalyst. The reversible transformation between A and B is critical for a partial oxidation process, but the transformation of B to C is undesirable and generally causes deactivation of the catalyst. This requires that the free energy change between A and B (ΔG_{A-B}) is small compared to that between B and C (ΔG_{B-C}). Unfortunately, in our system ΔG_{A-B} seems to be quite high so as to cause a fast transformation from OMS-1/OMS-2 to Mn_3O_4 and in some instances a transition all the way to MnO, as suggested by Krishnan and Suib (33).

Compared to studies reported by Krishnan and Suib (33), a more severe reducing environment is observed in this research because no O_2 was added to the feed for the reaction of 2-propanol decomposition. This may explain the quicker bulk-phase transformation of Cu–OMS-2 from cryptomelane to manganosite at 300°C, which is much lower than the 450°C used in studies reported by Krishnan and Suib (33).

4.3. In Situ FTIR Studies of the Adsorption of 2-Propanol over M–OMS-2 Materials

After the adsorption of 2-propanol, the spectra of Cu–OMS-2-I exhibit bands (1128 cm^{-1}) related to isopropoxide species, suggesting possible dissociative adsorption of 2-propanol. Bands (1570 and 1440 cm^{-1}) related to surface acetate species on Cu–OMS-2-I are also observed, even

at 120°C. This is probably because oxygen species on Cu–OMS-2-I are very active and can oxidize isopropoxide further to acetate species.

Compared to Cu–OMS-2-I, no distinctive bands relating to either isopropoxide or acetate species have been observed on Al–OMS-2 and OMS-2 after the adsorption of 2-propanol, suggesting that Cu–OMS-2-I has more active sites for 2-propanol on its surface than Al–OMS-2 and OMS-2. This is consistent with the conclusion that Cu–OMS-2 materials have much higher activity toward dehydrogenation of 2-propanol than other *M*–OMS-2 materials, according to the reaction results reported here. The active sites are probably due to defects introduced by the distorted CuO_6 octahedra in the framework, high Cu cation content in the tunnels of the cryptomelane structure of Cu–OMS-2 (as suggested by ICP-AES analysis (34), and/or active copper oxides on the surface of Cu–OMS-2 materials. The exact details of active sites still need to be determined. However, detailed studies of copper (and other) doped OMS-2 materials prepared by this synthetic route have shown that a combination of TEM (21), electrochemistry (21, 23, 24), and analytical elemental analyses (21, 23, 24) can be used to show that introduction of ions into the framework occurs when small amounts of dopant are added prior to reflux. Doping ions into tunnel sites occurs by ion exchange after the OMS-2 crystallizes during reflux.

V. CONCLUSIONS

There are no significant differences among conversions of 2-propanol for different *M*–OMS-2 materials, except for Cu–OMS-2 materials, which have much higher activity toward the decomposition of 2-propanol than other *M*–OMS-2 materials. Acetone is the major product with selectivities of 89 to 100% in reactions over *M*–OMS-2 materials. One of the other products is propene, which has selectivities generally below 6%. CO_2 was also detected during the reaction of 2-propanol over *M*–OMS-2 materials. Effects of different Cu contents in Cu–OMS-2 materials on the decomposition of 2-propanol were also studied. The conversion of 2-propanol grows with increasing Cu content in Cu–OMS-2 materials.

In a correlation of the reaction results for *M*–OMS-2 materials with acidity and basicity revealed by TPD studies for adsorbed NH_3/CO_2 (34), our results are consistent with the general idea that dehydration of 2-propanol happens on acidic sites and that dehydrogenation occurs on acid–base pair sites and redox centers. The redox properties of manganese ions in *M*–OMS-2-type materials appear to play a more significant role than acid–base properties in the high selectivity to acetone in the decomposition of 2-propanol over these *M*–OMS-2 catalysts.

XRD studies show that all synthesized *M*–OMS-2 materials have changed to the manganosite- (MnO-) type structure after reaction. Especially for Cu–OMS-2 materials, detailed XRD studies of phase transitions during reaction indicate that the bulk structure of the materials changes from cryptomelane (KMn_8O_{16}) to amorphous MnO_y ($1 \leq y \leq 2$), to hausmannite (Mn_3O_4), and finally to manganosite.

All Cu–OMS-2 materials that have either the cryptomelane, the amorphous MnO_y, the hausmannite, or the manganosite structure show activity in the decomposition of 2-propanol to acetone. The Cu–OMS-2 materials containing the hausmannite structure show the highest activity.

ACKNOWLEDGMENTS

We acknowledge the U.S. Department of Energy, Office of Basic Energy Science, Division of Chemical Sciences, and Texaco, Inc. for support of this research.

REFERENCES

1. Seo, K. T., Kang, S. C., Kim, H. J., and Moon, S. K., *Kor. J. Chem. Eng.* **2**, 163 (1985).
2. Grzybowska-Swierkosz, B., *Mater. Chem. Phys.* **17**, 121 (1987).
3. Ai, M., and Suzuki, S., *J. Catal.* **30**, 362 (1973).
4. Ai, M., *J. Catal.* **40**, 327 (1975).
5. Ai, M., *J. Catal.* **49**, 305 (1977).
6. Noller, H., Lercher, J. A., and Vinek, H., *Mater. Chem. Phys.* **18**, 577 (1988).
7. Orita, H., Hayakama, T., Shimizu, M., and Takehira, K., *Appl. Catal.* **71**, 133 (1991).
8. Gervasini, A., and Auroux, A., *J. Catal.* **121**, 190 (1991).
9. Petrakis, D. E., Pomonis, P. J., and Soudkos, A. T., *J. Chem. Soc. Faraday Trans.* **81**, 86 (1991).
10. Niyama, H., and Echigoya, E., *Bull. Chem. Soc. Jpn.* **44**, 1739 (1971).
11. Miyata, H., Kohno, M., Ono, T., Ohno, T., and Hatayama, F., *J. Mol. Catal.* **63**, 181 (1990).
12. Hathaway, P. E., and Davis, R. J., *J. Catal.* **116**, 279 (1989).
13. McKenzie, A. L., Fishel, C. T., and Davis, R. J., *J. Catal.* **138**, 547 (1992).
14. Pepe, F., Angelotti, L., and De Rossi, S., *J. Catal.* **118**, 1 (1989).
15. Tanabe, K., Misono, M., Ono, Y., and Hattori, H., "New Solid Acids and Bases." Elsevier, Amsterdam, 1989.
16. Yashima, T., Suzuki, H., and Hara, N., *J. Catal.* **33**, 486 (1974).
17. Rekoske, J. E., and Barteau, M. A., *J. Catal.* **165**, 57 (1997).
18. Wang, J. A., Bokhimi, X., Novaro, O., Lopez, T., Tzompantzi, F., Gomez, R., Navarrete, J., Llanos, M. E., and Lopez-Salinas, E., *J. Mol. Catal. A* **137**, 239 (1999).
19. Matsuo, K., Nitta, M., and Aomura, K., *J. Catal.* **54**, 446 (1978).
20. Matsuo, K., Nitta, M., and Aomura, K., *J. Jpn. Pet. Inst.* **19**, 745 (1976).
21. Shen, Y. F., Suib, S. L., and O'Young, C. L., *J. Am. Chem. Soc.* **116**, 11020 (1994).
22. DeGuzman, R. N., M.S. thesis, The University of Connecticut, Storrs, CT, 1994.
23. DeGuzman, R. N., Shen, Y. F., Suib, S. L., Shaw, B. R., and O'Young, C. L., *Chem. Mater.* **5**, 1395 (1993).
24. DeGuzman, R. N., Shen, Y. F., Neth, E. J., Suib, S. L., O'Young, C. L., Levine, S., and Newsam, M., *Chem. Mater.* **6**, 815 (1994).
25. Shen, Y. F., Zerger, R. P., DeGuzman, R. N., Suib, S. L., McCurdy, L., Potter, D. I., and O'Young, C. L., *J. Chem. Soc. Chem. Commun.* 1213 (1992).
26. Shen, Y. F., Zerger, R. P., DeGuzman, R. N., Suib, S. L., McCurdy, L., Potter, D. I., and O'Young, C. L., *Science* **260**, 511 (1993).
27. Suib, S. L., and Iton, L. E., *Chem. Mater.* **6**, 429 (1994).
28. Shen, Y. F., Suib, S. L., and O'Young, C. L., *J. Catal.* **161**, 115 (1996).

29. Xia, G. G., Yin, Y. G., Willis, W. S., Wang, J. Y., and Suib, S. L., *J. Catal.* **185**, 91 (1999).
30. Zhou, H., Shen, Y. F., Wang, J. Y., Chen, X., O'Young, C. L., and Suib, S. L., *J. Catal.* **176**, 321 (1998).
31. Zhou, H., Wang, J. Y., Chen, X., O'Young, C. L., and Suib, S. L., *Microporous Mesoporous Mater.* **21**, 315 (1998).
32. Wang, J. Y., Xia, G. G., Yin, Y. G., Suib, S. L., and O'Young, C. L., *J. Catal.* **176**, 275 (1998).
33. Krishnan, V. V., and Suib, S. L., *J. Catal.* **184**, 305 (1999).
34. Chen, X., Shen, Y. F., Suib, S. L., and O'Young, C. L., in preparation.
35. Potter, R. M., *Am. Miner.* **64**, 1199 (1979).
36. Kooli, F., Martin, C., and Rives, V., *Langmuir* **13**, 2303 (1997).
37. O'Young, C. L., Sawicki, R. A., Shen, Y. F., and Suib, S. L., U.S. Patent 5,523,509, 1996.
38. Miyata, H., Tokuda, S., Ono, T., and Hatayama, F., *J. Chem. Soc. Faraday Trans.* **81**, 86 (1990).
39. Chen, X., Ph.D. thesis, The University of Connecticut, Storrs, CT, 2000.
40. Nelson, D. L., and Webb, B. P., *in* "Encyclopedia of Chemical Technology" (Kirk-Othmer, Ed.), 4th ed., Vol. 1, p. 184. Wiley, New York, 1991.
41. Owen, O. S., and Kung, H. H., *J. Mol. Catal.* **79**, 265 (1993).
42. Vanysek, P., *in* "CRC Handbook of Chemistry and Physics" (R. C. Weast, M. J. Astle, and W. H. Beyer, Eds.), 67th ed., p. D-151. CRC Press, Boca Raton, FL, 1986.
43. Aboukais, A., Bechara, R., Aissi, C. F., Bonnelle, J. P., Ouqour, A., Loukah, M., Coudurier, G., and Vedrine, J. C., *J. Chem. Soc. Faraday Trans.* **89**, 2545 (1993).
44. Lahousse, C., Bachelier, J., Lavalley, J. C., Lauron-Pernot, H., and Le Govic, A. M., *J. Mol. Catal.* **87**, 329 (1994).
45. Grzybowska-Swierkosz, B., Coudurier, G., Vedrine, J. C., and Gressel, I., *Catal. Today* **20**, 165 (1994).
46. Mars, P., and van Krevelen, D. W., *Chem. Eng. Sci.* **3**, 41 (1954).
47. Kung, H. H., and Kung, M. C., *Adv. Catal.* **79**, 265 (1993).
48. Nicolas-Tolentino, E., Tian, Z. R., Zhou, H., Xia, G. G., and Suib, S. L., *Chem. Mater.* **11**, 1733 (1999).